Article

Current Biology

Vagus nerve stimulation induces widespread cortical and behavioral activation

Highlights

- VNS induces behavioral changes associated with increased arousal state in mice
- VNS induces widespread excitation of the cortex
- VNS activates cholinergic and noradrenergic fibers in the cortex
- VNS-induced cortical activation cannot be explained by motor activity alone

Authors

Lindsay Collins, Laura Boddington, Paul J. Steffan, David McCormick

Correspondence

davidmc@uoregon.edu

In brief

Collins et al. investigate the role of vagus nerve stimulation (VNS) on arousal state in mice. Results indicate that VNS reliably increases behavioral measures of arousal, including pupil dilation and locomotion. Moreover, VNS leads to widespread activation of excitatory neurons as well as cholinergic and noradrenergic axons in the cortex.

Collins et al., 2021, Current Biology *31*, 2088–2098
May 24, 2021
https://doi.org/10.1016/j.cub.2021.02.049

CellPress

CellPress

Current Biology

Article

Vagus nerve stimulation induces widespread cortical and behavioral activation

Lindsay Collins,[1,2] Laura Boddington,[1,2] Paul J. Steffan,[1] and David McCormick[1,3,*]
[1]Institute of Neuroscience, University of Oregon, Eugene, OR 97401, USA
[2]These authors contributed equally
[3]Lead contact
*Correspondence: davidmc@uoregon.edu
https://doi.org/10.1016/j.cub.2021.02.049

SUMMARY

Vagus nerve stimulation (VNS) is used for management of a variety of neurological conditions, although the therapeutic mechanisms are not fully understood. Accumulating evidence suggests that VNS may modulate cortical state and plasticity through activation of broadly projecting neuromodulatory systems. Using a mouse model, we compared arousal-linked behaviors with dorsal cortical activity obtained with widefield and two-photon GCaMP6s calcium imaging and electrophysiological recordings. We observed robust and reliable cortical and behavioral dose-dependent activation in waking mice to VNS, including pupil dilation and, frequently, whisker movements and locomotion. Widefield calcium imaging and multiunit recording during VNS revealed that this observed increase in arousal state is coupled with a rapid and widespread increase in excitatory activity, including, but not limited to, activation of somatosensory, visual, motor, retrosplenial, and auditory cortical regions. Two-photon GCaMP6s calcium imaging of cholinergic and noradrenergic cortical axons revealed that VNS strongly activates these neuromodulatory systems. Importantly, VNS-evoked activation of neuromodulatory axons and excitatory neurons in the cortex persisted in mice under light anesthesia, in the absence of overt movement. Arousal state changes were abolished by vagus nerve transection, confirming that observed VNS effects were specific to nerve stimulation and triggered widespread activity above that which can be explained by motor activity. Taken together, our results support a model of VNS in which activation of subcortical structures leads to widespread activation of cortex and an increase in arousal state, at least partially due to the activation of cholinergic and noradrenergic modulatory pathways.

INTRODUCTION

Stimulation of the vagus nerve is widely used as a treatment for epilepsy, depression, and migraine[1–4] and is under investigation as a method to drive or enhance plasticity in pathological conditions, such as tinnitus and motor impairment following stroke.[5,6] Despite vagus nerve stimulation (VNS) being FDA-approved for treatment of epilepsy for over 20 years,[7] little is known about the rapid physiological effects of VNS in the brain.

VNS has been shown to evoke simultaneous activity in many brain regions,[8,9] suggesting a role for activation of far-reaching projections, a hallmark of neuromodulatory systems. Indeed, short bursts of VNS dose-dependently drive activity in the noradrenergic locus coeruleus (LC),[10] and chronic VNS can lead to increased LC basal firing rates.[11] Although understanding of cholinergic activation is more limited, electrical stimulation of the vagus nerve also activates basal forebrain structures with dense cholinergic cell populations[12,13] and modulates cortical synchrony through activation of muscarinic receptors.[14] Noradrenaline (NA) and acetylcholine (ACh) modulate cortical activity and excitability (see Rho et al.[15] for review) and therefore are promising candidates to participate in the underlying widespread changes in cortical activity resulting from VNS.

The basal forebrain cholinergic and LC noradrenergic modulatory pathways are tightly linked to the regulation of arousal state and the structure of forebrain activity. For example, in monkeys, LC firing rate increases immediately preceding pupil dilation, a reliable indicator of arousal state.[16] In mice, pupil dilation and constriction rapidly track fluctuations in both noradrenergic and, to a lesser extent, cholinergic axon activity in the cortex.[17] Arousal state or sleep disturbances occur across many forms of epilepsy, depression, and migraine,[18–20] conditions for which VNS has been found to be a useful treatment option. Because VNS appears to influence these same neuromodulatory systems that are strongly linked to changes in arousal state, it is possible that the therapeutic effects of VNS could be partially explained by the modulation of arousal and brain state.[21]

Here, we take advantage of recent evidence that the internal brain state and general arousal level in mice can be reliably indexed not only by changes in pupil diameter and locomotion[22] but also orofacial movements[23–25] to determine the extent to which VNS alters arousal, behavioral, and brain state. We demonstrate that VNS dose dependently increases arousal and behavioral state and induces widespread but non-uniform cortical activation as well as activation of neuromodulatory noradrenergic and cholinergic systems. We find that VNS effects

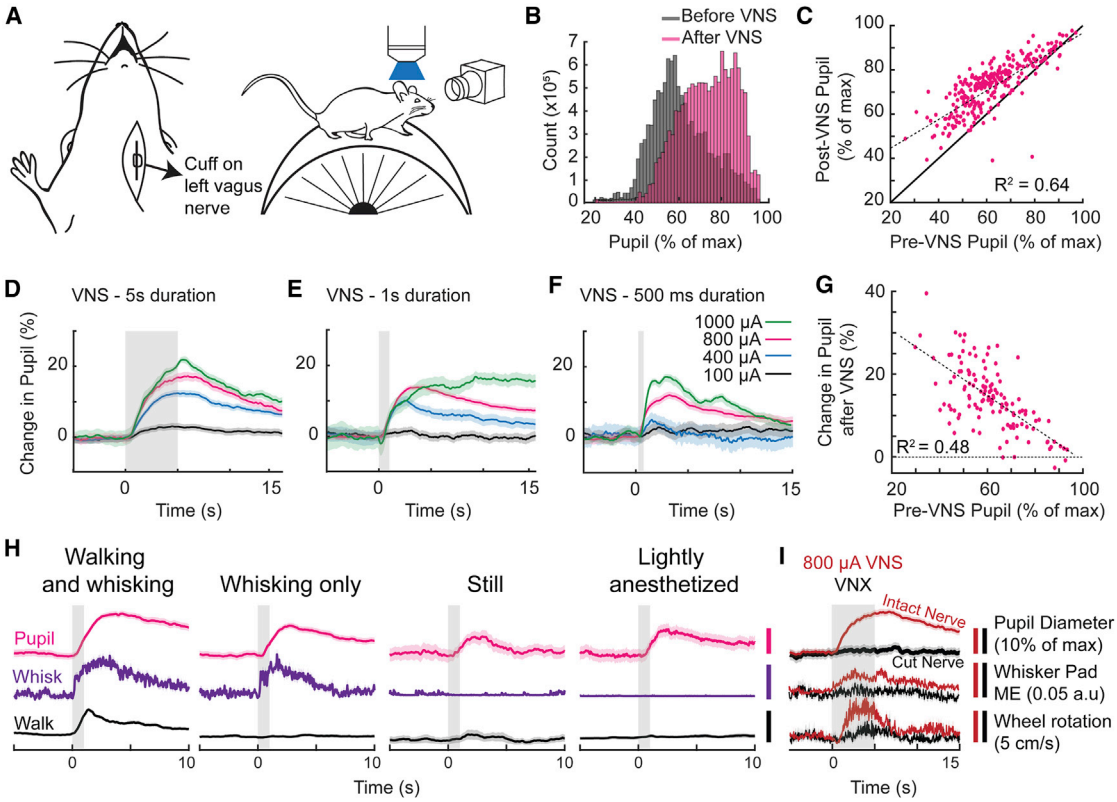

Figure 1. Vagus nerve stimulation triggers an increase in arousal state

(A) Left: schematic of vagus nerve cuff position. Right: schematic of a mouse on wheel with overhead objective for brain imaging and side camera for face video capture is shown.

(B) Distribution of pupil diameter for 2 s preceding VNS (gray) and 2 s immediately after VNS onset (magenta; N = 8 mice, n = 281 stimulations). Pupil diameter is presented as percent of maximum pupil diameter in each recording. Data are shown from 800 μA VNS applications of 1-s duration with 800 μs pulse width.

(C) Average pupil diameter during the 1 s after VNS offset as a function of average pupil diameters during the 1 s before VNS onset (N = 8 mice, n = 281 stimulations). Same data as (B) are shown.

(D) Change in pupil diameter over time after increasing intensities of 5 s of VNS (for 100 μA: N = 6 mice, n = 120 stimulations; for 400 μA: N = 6 mice, n = 185 stimulations; for 800 μA: N = 8 mice, n = 163 stimulations; for 1,000 μA: N = 2 mice, n = 16 stimulations). VNS parameters were applied in blocks of identical stimulation, and traces include trials for all behavioral states pooled.

(E) Same as (D) with 1-s duration VNS (for 100 μA: N = 4 mice, n = 48 stimulations; for 400 μA: N = 5 mice, n = 58 stimulations; for 800 μA: N = 8 mice, n = 281 stimulations; for 1,000 μA: N = 2 mice, n = 17 stimulations).

(F) Same as (D) with 500-ms duration VNS (for 100 μA: N = 2 mice, n = 33 stimulations; for 400 μA: N = 2 mice, n = 36 stimulations; for 800 μA: N = 2 mice, n = 210 stimulations; for 1,000 μA: N = 2 mice, n = 20 stimulations).

(G) Change in pupil diameter after 800 μA, 1 s VNS as a function of pre-VNS pupil diameter (N = 6 mice, n = 136 stimulations). Change in pupil is defined as the difference between the maximum pupil diameter recorded during the 2 s after VNS onset and the mean pupil diameter during 2 s before onset.

(H) Pupil responses to VNS separated by behavioral state (N = 8 mice). From left to right: walking accompanied by whisker pad movement (n = 48 stimulations), whisker pad movement only (n = 94 stimulations), behaviorally still with no overt whisker pad movement or wheel movement (n = 20 stimulations), and lightly anesthetized (N = 3 mice, n = 80 stimulations) is shown. Scale bars are same as shown in (I).

(I) Behavioral responses to VNS before (black) and after (red) nerve transection (N = 3 mice, n = 163 intact stimulations, 77 VNX stimulations).

Figure S1 provides additional analysis of data presented in this figure. All error bars represent SEM.

are state dependent, where the preceding brain state influences the extent to which VNS alters arousal, movement, and brain activity.

RESULTS

Influence of VNS on arousal

The internal arousal state of mice was assessed through measurements of pupil diameter, whisker pad movement, and walking speed as assessed by wheel movement (STAR Methods). Mice were head fixed atop a running wheel while pupil and facial movements were monitored from a lateral view (Figure 1A). Unless otherwise stated, walking is defined as wheel rotational velocity exceeding 2.5 cm/s to capture both running bouts and pronounced limb movement. VNS consistently increased pupil diameter (Figures 1B, 1C, S1A, and S1B) in a dose-dependent manner (Figures 1D–1F), where higher amplitude or longer duration VNS induced large pupil responses (Figure 1D) and smaller doses of VNS induced slightly smaller pupil dilations (Figure 1F). VNS trains of 1 and 5 s duration and greater than 400-μA stimulation induced a significant increase in pupil diameter compared to baseline during the 6 s following

stimulation onset (stimulation duration and amplitude: 5 s, 400 μA: change of 16.4% ± 1.0%, $F_{6,1267}$ = 35.27, p < 0.0001; 5 s, 800 μA: change of 16.0% ± 0.93%, $F_{6,1134}$ = 36.8, p < 0.0001; 5 s, 1,000 μA: change of 21.5% ± 1.06%, $F_{6,105}$ = 28.0, p < 0.0001; 1 s, 400 μA: change of 13.1% ± 0.93%, $F_{6,399}$ = 5.94, p < 0.01; 1 s, 800 μA: change of 18.9% ± 0.70%, $F_{6,1946}$ = 58.73, p < 0.0001; 1 s, 1,000 μA: change of 17.4% ± 2.34%, $F_{6,105}$ = 28.0, p < 0.01). VNS trains of 500-ms duration only induced significant increases in pupil diameter with stimulation intensities greater than 800 μA (500 ms, 800 μA: change of 14.5% ± 0.70%, $F_{6,1461}$ = 15.15, p < 0.0001; 500 ms, 1,000 μA: change of 18.13% ± 1.56% $F_{6,133}$ = 21.18, p < 0.0001).

Pupil responses to VNS were dependent upon the state of the animal at the time of stimulation (Figure S1C), resulting in a strong and significant negative correlation between the change in pupil diameter evoked by VNS and the pre-VNS pupil diameter (Figure 1G; Pearson's r = −0.69; p < 0.0001; R^2 = 0.48).

VNS often, but not always, initiated both whisker pad movement and wheel movement (which could be either locomotion or non-locomotion-related limb movements; Figure 1). Higher intensity stimulations were more likely to elicit a pupil dilation or bout of whisking or wheel movement (Figures S1D–S1F). Pupil diameter has been shown to be highly correlated with whisking and locomotive behaviors.[24,25] Therefore, to ensure that VNS-evoked pupil dilation was not simply due to the associated whisker pad or limb movement noted on some trials, trials where whisker pad and/or wheel movement were not detected were separated. A smaller but consistent effect on pupil dilation remained (Figure 1H), indicating that VNS-induced pupil dilation can be independent of dilations associated with these types of movements. This effect was further confirmed in lightly isoflurane-anesthetized mice where VNS continued to evoke pupil dilation in the absence of any detectable whisker pad movement or wheel rotation (Figure 1H). All arousal responses to VNS were abolished after combined proximal and distal (to the stimulation cuff) transection of the vagus nerve (VNX) (Figures 1I, n = 3, and S1G), confirming that the observed effects required conduction through the vagus nerve and that off-target stimulation was not driving increases in activation and arousal.

Widespread cortical activation during VNS

We hypothesized that VNS would trigger widespread cortical activation that may be observed using widefield GCaMP6s imaging. Using one-photon epifluorescence widefield imaging in Thy1-GCaMP6s mice, which express GCaMP6s throughout excitatory neurons in the cerebral cortex (see Salkoff et al.[24]), we were able to quantify the extent to which VNS activated cortical excitatory cells in broad dorsal cortical regions (Figure 2A). Mice were positioned on the running wheel beneath a widefield camera, and VNS was applied with an interstimulus interval of between 30 and 90 s. This interval was chosen after preliminary evidence demonstrated that widefield measures always returned to baseline by 30 s after VNS (mean = 3.68 ± 3.75 s; max = 20.9 s; Figure S2A).

Application of VNS evoked arousal state increases (Figure S1B) and a dose-dependent increase in GCaMP6s cortical fluorescence with higher intensity and longer pulse width stimulation resulting in a larger, longer lasting increase (Figure 2B). A widespread, bilateral increase in GCaMP6s calcium signaling was observed across the dorsal surface of the brain (Figure 2C; Video S1). VNS-evoked cortical GCaMP6s activation was also consistently greater than activation resulting from spontaneous motor activity alone (i.e., no VNS; Figure 2D). We observed no significant difference in VNS response between homologous regions in the two hemispheres (Figures 2E and S2C). The magnitude and spread of this activation were dependent on the evoked behavioral state change of the animal. VNS applications that triggered walking induced the largest change in calcium activity compared to applications that evoked whisking only (Figures 2C and S2D). Under light isoflurane anesthesia, much of the cortical response was maintained, even in the absence of overt movement (Figure 2C).

Spatial spread of cortical activation was measured by separately analyzing identified regions of the dorsal cortical surface bilaterally (including motor, somatosensory, visual, and retrosplenial areas; using the Allen Institute common coordinate framework [CCF]). All regions measured exhibited stimulus-locked increases in GCaMP6s fluorescence, both during trials that evoked wheel or whisker pad movement and those in which the animal remained still under isoflurane anesthesia (Figures 2E and S2E). Responses tended to initiate medially at the confluence of the somatosensory, motor, and retrosplenial regions on the dorsal surface and spread outward (Figures 2F and S2F). When compared to the CCF, this peak of activation appeared to be centered within the lower body/limb area of the somatosensory cortex (Figure 2C). A similar pattern was observed during VNS applications that induced walking and whisking behaviors and those that were recorded under isoflurane anesthesia, although the magnitude of calcium responses during trials that evoked wheel movement was substantially greater (Figure 2F).

A separate group of mice were implanted with headposts allowing for lateral widefield imaging of the right auditory and barrel cortical regions (Figure 2G; Video S2). A strong VNS-induced activation was observed in both regions (Figure 2H). Activation was significantly greater during trials in which VNS evoked walking or whisking behaviors than in trials performed under isoflurane anesthesia (Figure S2E). VNS-induced responses were consistently greater compared to spontaneous periods of still, whisking, and/or walking (Figure S2G).

Changes in reflected cortical fluorescence of GCaMP6s signaling are contaminated by changes in blood flow and other intrinsic signals.[26] To examine the influence of these non-Ca^{2+}-dependent signals, we alternatively (every other frame) imaged with blue and green LEDs. Subtraction of the non-Ca^{2+}-dependent signal (green LED illumination) from that obtained with the blue LED resulted in a slight reduction in the peak amplitude of the measured GCaMP6s responses. Overall hemodynamic subtraction did not substantially alter the shape or timing of the responses across regions, with the exception of the auditory cortical region, where large blood vessels in this area appeared to contaminate the peak and duration of the GCaMP6s signals (Figure S2H). The finding that hemodynamic changes accompany cortical excitation in response to VNS was supported by a small examination of blood vessel dilation using two-photon imaging (Figure S2I; Video S3). Blood vessel dilations were stimulus locked but delayed by about 1–1.5 s from stimulation onset.

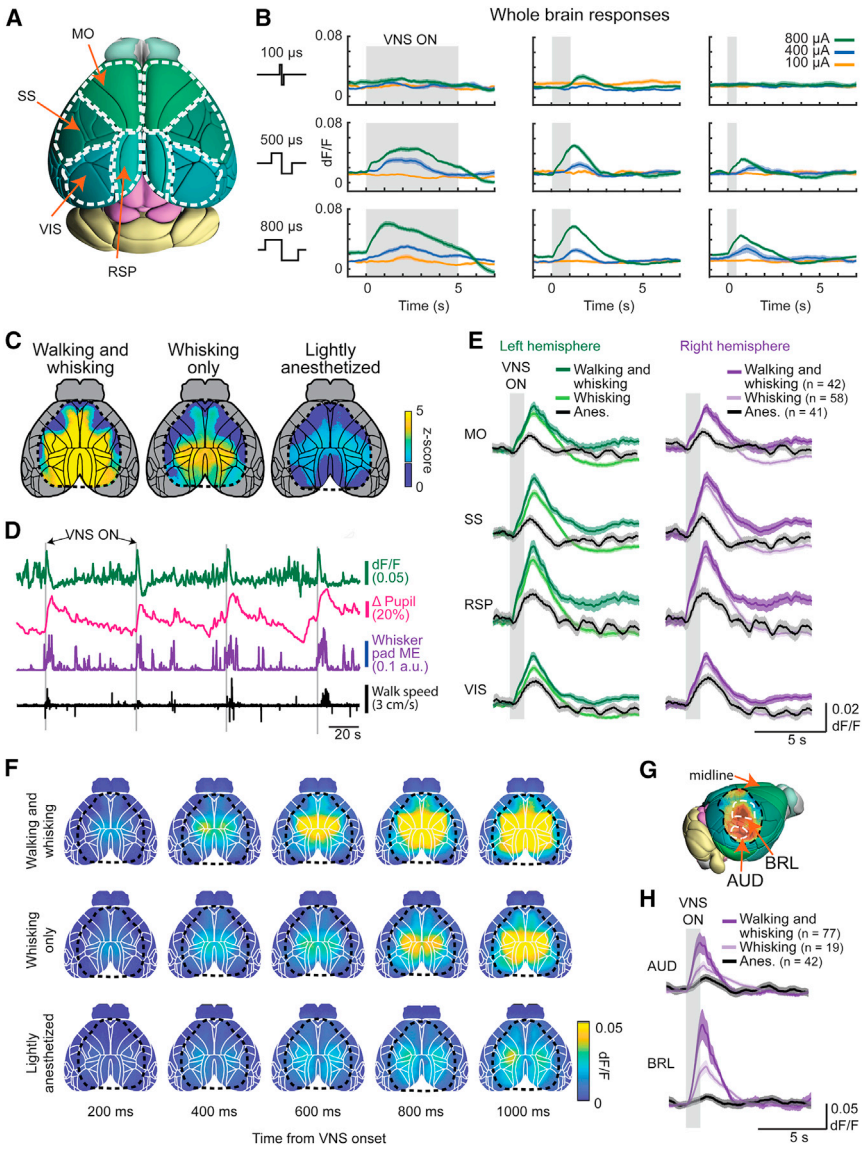

Figure 2. VNS triggers widespread cortical activation

(A) Allen Institute Common Coordinate Framework (CCF) map of the mouse cortex dorsal surface. Dotted areas were selected for regional analysis. MO, motor; RSP, retrosplenial; SS, somatosensory; VIS, visual.

(B) VNS led to a dose-dependent increase in GCaMP6s signaling across the dorsal surface. Longer pulse widths of VNS (top to bottom), longer durations of VNS (left to right; gray bars indicate time of VNS application), and increased amplitude of VNS led to larger increases in dF/F (N = 2 mice, n = 25–44 stimulations). Traces include trials for all behavioral states pooled.

(C) VNS-evoked change in excitatory neuronal/neuropil activity in the dorsal cortex during the 1 s of VNS application (N = 4 mice) divided into trials that triggered (left to right) wheel movement accompanied by whisking (n = 42 stimulations), orofacial movement only (n = 58 stimulations), and no observed movement under light isoflurane anesthesia (n = 41 stimulations). Color represents deviation from pre-VNS baseline, calculated as mean dF/F for each pixel during 1 s preceding VNS onset.

(D) Example raw traces of dF/F (green), pupil diameter (magenta), whisker pad movement (purple), and wheel rotation (black). Gray bars indicate VNS.

(E) VNS evokes a sharp increase in GCaMP6s fluorescence across both hemispheres in all regions examined. The largest activation occurs after VNS applications that evoke wheel and orofacial movement. Activation was maintained in isoflurane-anesthetized mice, although the response was significantly lessened in all areas except visual cortex (Figure S2E). Data displayed are mean ± SEM.

(F) Heatmaps of widefield imaging of GCaMP6s fluorescence over 1 s of VNS application separated by behavioral state (same data from C).

(G) CCF map of the mouse cortex lateral surface. Black dotted line represents area recorded during widefield imaging. Analyses were performed on right auditory (AUD) and barrel (BRL) cortices during VNS (white dotted lines; N = 2 mice).

(H) VNS evoked a large increase in GCaMP6s signaling in both auditory and barrel cortical areas that was significantly greater in trials that evoked wheel or whisker pad movement (Figure S2E). Data displayed are mean ± SEM.

Figure S2 provides additional analyses of data presented in this figure. See also Videos S1, S2, andS3.

Mechanisms underlying VNS-evoked arousal state changes

A separate series of experiments was conducted to test for potential circuit mechanisms underlying the VNS-evoked changes we observed. First, we tested whether cortical activation observed in widefield experiments is associated with activation of layer 2/3 excitatory neurons. Widefield imaging from Thy1-GCaMP6s mice captures combined fluorescence signals from both cell bodies and neuronal processes in superficial cortical layers,[27] so we performed two-photon imaging of cell bodies in layer 2/3 to minimize neuropil contamination. Second, we tested whether noradrenergic and cholinergic axons in cortex are activated by VNS and whether or not this was dependent upon motor responses.

Activation of excitatory neurons in cortex

A CamKII-tetO-GCaMP6s mouse line was used due to high expression of GCaMP6s in excitatory neuronal somata.[28] Cells within the ''hotspot'' zone of highest response to VNS (determined by widefield imaging) were imaged using a two-photon microscope (ThorLabs Mesoscope; Figure 3A). Using two-photon imaging, we were able to simultaneously monitor between 40 and 302 cell bodies during VNS in the hotspot (typically in the lower limb area of somatosensory cortex). VNS evoked strong increases in the average somatic GCaMP6s signal within the imaged region. This increase in neuronal activity was associated with VNS-evoked whisking, wheel movement, and pupil dilation. Whisking and neuronal activity initiation preceded wheel movement and pupil dilation

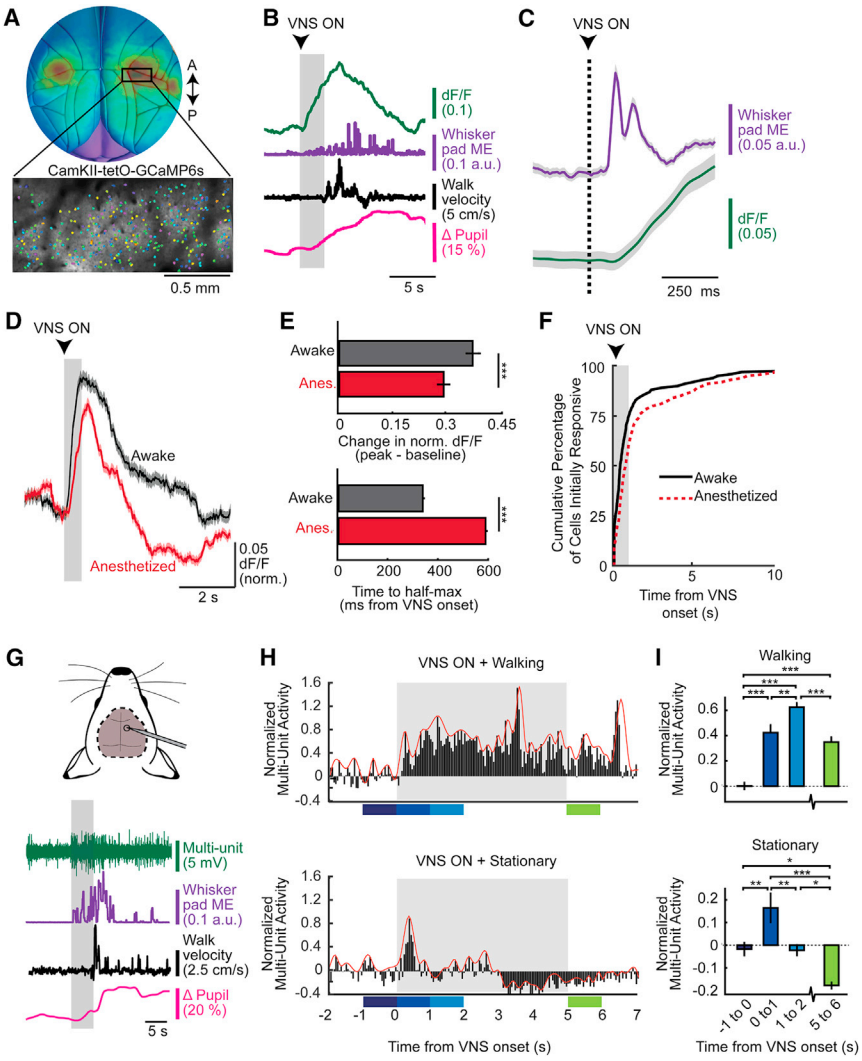

Figure 3. Cortical excitatory neuron response to VNS

(A) Top: cortical response to VNS was determined using widefield imaging (response shown overlaid on the Allen Institute CCF). Regions of interest (ROIs) were selected within the region of largest VNS response for two-photon imaging through a circular cranial window. Bottom: colored cells are those detected by Suite2P image analysis software.

(B) Representative example of VNS-evoked changes in GCaMP6s fluorescence (dF/F) averaged across all cells recorded during a single application of VNS relative to behavioral measures of pupil diameter, whisker pad motion, and wheel movement.

(C) Averaged whisking and dF/F data across all cells during all awake trials showed that, on average, whisking and calcium activity rise with a similar time course.

(D) Averaged dF/F responses to VNS while awake (black; N = 3 mice, n = 1,285 cells, n = 156 stimulations) and lightly anesthetized (red; N = 2 mice, n = 668 cells, n = 77 stimulations). Individual cell responses to VNS are shown in Figure S3.

(E) Compared to anesthetized trials, VNS delivered during awake trials induced a greater magnitude (top) and faster (bottom) change in normalized dF/F on average.

(F) Cumulative percentage of cells initially responsive to VNS during awake (solid black line) and anesthetized (dotted red line) recordings across time.

(G) Top: multiunit recordings were obtained from the dorsal cortical area that maximally responded to VNS, determined by widefield imaging. Bottom: representative example of one VNS application is shown.

(H) Multiunit activity recorded during VNS when still (n = 72 stimulations) and when VNS evoked wheel movement (n = 35 stimulations; N = 5 mice). Data are presented relative to pre-VNS baseline spike rate, defined as the mean number of spikes recorded during the 1 s preceding VNS onset. Peak upper envelope overlaid in red.

(I) Normalized multiunit activity, as shown in (H) during 1-s bins surrounding VNS onset. Colors and timing of bins correspond to marked areas in (H).

*p < 0.05; **p < 0.01; ***p < 0.001. Error bars represented as SEM in all panels. See also Figure S3.

(representative example shown in Figure 3B). Across all averaged trials, calcium activity began to rise within 200 ms following onset of VNS, a time course that is similar to whisking activity (Figure 3C). This pattern of neuronal activation was consistent across all stimulations and complements results from widefield imaging.

We then compared activity during awake stimulations and stimulations administered during light isoflurane anesthesia (Figure 3D). Stimulation evoked an increase in average activity in both awake and anesthetized states; however, fluorescence increased significantly more (mean peak to baseline change in normalized dF/F while awake: 0.379 ± 0.017; anesthetized: 0.297 ± 0.017; t = 4.230; p < 0.0001; Student's t test) and rose significantly faster in the awake state compared to lightly anesthetized (mean time to half-max normalized dF/F while awake: 333.53 ± 2.52 ms; anesthetized: 582.53 ± 12.355 ms; t = −11.973; p < 0.0001; Student's t test; Figure 3E). To quantify the timing of cell recruitment following VNS application, we determined the time at which each cell was initially responsive to VNS, defined as 2 times the baseline dF/F (baseline calculated as mean dF/F during 2 s preceding VNS). Recruitment occurred more quickly in the awake state (mean latency to respond = 333.53 ± 0.25 ms) compared to anesthetized (mean latency to respond = 582.53 ± 1.24 ms; k = 0.530; p < 0.0001; two-sample Kolmogorov-Smirnov test; Figure 3F).

In addition to monitoring neural activity with GCaMP6 imaging, we performed extracellular multiunit recordings of layer 2/3 cortical neurons during VNS within the region most strongly activated by VNS, as determined by widefield imaging (Figure 3G). VNS-evoked stimulus artifacts were blanked, and action potentials were detected using custom MATLAB software. Normalized multiunit activity is presented here as change from pre-VNS baseline, defined as average spike rate during the 1 s before VNS onset. During both walking and stationary trials, VNS led to a rapid increase in firing

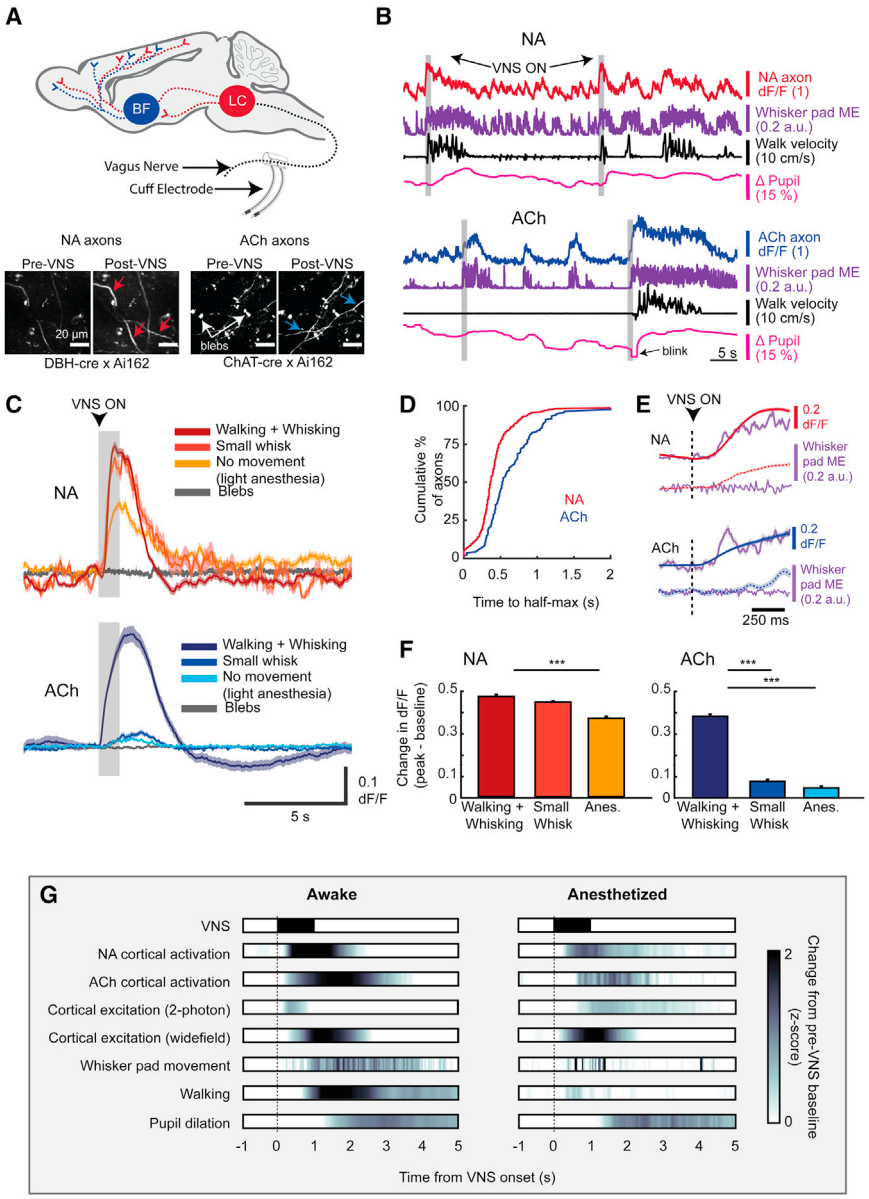

Figure 4. Noradrenergic and cholinergic response to VNS

(A) Top: schematic illustrating the pathway from the vagus nerve through the LC and basal forebrain to the cortex. Bottom: micrographs show example two-photon images of NA axons (left; red arrows) and ACh axons (right; blue arrows) in superficial cortex. Pre-VNS images are averaged over all frames collected during the 2 s before VNS onset, and post-VNS images are frames averaged over 2 s after VNS onset. Auto-fluorescent blebs (white arrows) were used to determine possible effects of motion on imaging results.

(B) Representative traces from an NA (top) and ACh (bottom) axonal imaging session.

(C) Top: averaged response of all recorded NA axons (n = 40 axon segments, n = 131 stimulations, N = 1 mouse) to VNS. Bottom: averaged response of all recorded ACh axons (n = 68 axon segments, n = 258 stimulations, N = 3 mice) to VNS is shown. Corresponding behavioral data are shown in Figures S4A and S4B.

(D) Cumulative percentage of NA axons (red) and ACh axons (blue) reaching half of maximum GCaMP6s dF/F over time.

(E) Early NA axon (top) and ACh axon (bottom) and whisking response to VNS. Solid lines represent axon responses during trials that evoked whisking, and dotted lines depict axon responses to trials that did not elicit any movement. Averaged whisking traces are shown in purple.

(F) VNS-evoked change in dF/F for NA axons (left) and ACh axons (right) for stimulations that evoked wheel movement, whisking, or stimulations applied under light anesthesia. ***$p < 0.001$.

(G) Timing of responses to VNS. Data are combined from awake (left) and anesthetized (right) experiments and presented as variation (*Z* score) from pre-VNS baseline (average activity during 5 s before stimulation). Behavioral data are taken from widefield experiments.

All error bars represent SEM. See also Figure S4.

rate that peaked 250 ms (walking trials) or 350 ms (stationary trials) after stimulus onset (Figure 3H). To assess the persistence in this increase in firing rate, data were split into 1-s epochs relative to stimulation onset (Figure 3I). When stationary, the increased multiunit activity consistently occurred during the first 1-s epoch following VNS onset (16.48% ± 6.36% change; $F = 14.15$; $p < 0.0001$; one-way ANOVA with post hoc multiple comparison testing) and returned to baseline levels by the second epoch, even though the VNS train was still ongoing (−2.22% ± 2.3% change; $p = 0.54$). A significant reduction in multiunit activity occurred during the epoch spanning 5 to 6 s after VNS onset (−17.79% ± 1.35% change; $p < 0.05$). In trials in which VNS initiated walking, increased multiunit activity was observed in the first second after VNS onset (42.30% ± 6.03% change, $F = 38.10$; $p < 0.0001$, one-way ANOVA with post hoc multiple comparison testing) and persisted through the VNS application (1 to 2 s following VNS onset: 62.42% ± 3.36% change, $p < 0.0001$) and remained high after VNS offset (5 to 6 s following VNS onset: 34.81% ± 4.00% change, $p < 0.0001$).

VNS activation of neuromodulatory systems

We hypothesized that noradrenergic and cholinergic neuromodulatory systems may also be activated by VNS and therefore play a role in increasing cortical activity. We tested this hypothesis by imaging GCaMP6s expressed in cortical NA or ACh axons during VNS (Figure 4A). As reported previously,[29,30] increases in activity of both NA and ACh axons were highly correlated with behavioral indicators of arousal (Figure 4B). VNS also resulted in strong increases in GCaMP6s fluorescence in both NA and ACh axons within the dorsal cerebral cortex (Figure 4C). NA activity rose more quickly than ACh, with ~75% of axons reaching half-max dF/F within 0.5 s, compared to ~50% of ACh axons (Figure 4D). Rise in ACh activity was also more

dependent on the initiation of whisker movement following VNS. In trials that evoked whisking, both NA and ACh axons responded with a similar time course as the whisking behavior. However, in the absence of VNS-induced whisking, NA maintained a strong response to VNS, whereas the response in ACh axons was significantly diminished (Figure 4E).

Even in trials that evoked no discernable locomotor activity, with small movements of the whiskers, an increase in NA signaling persisted in response to VNS ($t = 14.46$; $p < 0.0001$; Student's t test). ACh signaling also increased when VNS triggered only small whisker pad movements ($t = 4.31$; $p < 0.0001$; Student's t test), although the magnitude was substantially diminished in comparison to responses occurring during strong whisker pad movements/locomotion (Figure 4C). To completely remove any contribution of motor-related activity to NA and ACh signals, we lightly anesthetized mice with isoflurane. In the anesthetized condition, both the NA and ACh responses were reduced, but a significant response remained compared to pre-VNS baseline (NA: $t = 14.94$, $p < 0.0001$; ACh: $t = 5.38$, $p < 0.0001$, Student's t test). We calculated the magnitude of the change in fluorescence by subtracting the mean dF/F during the 2 s preceding VNS onset from the maximum dF/F during the 2 s following VNS onset. One-way ANOVAs with multiple comparison pairwise post hoc tests were performed to test for significance between groups. A significant group effect was found for both NA ($F_{2,558} = 32.41$; $p < 0.0001$) and ACh axonal responses ($F_{2,173} = 58.84$; $p < 0.0001$). VNS-aligned change in NA signaling during small whisk trials (mean = 0.47 ± 0.005) did not significantly differ from those which evoked wheel movement (mean = 0.49 ± 0.0007; $p = 0.91$; Figures 4C and 4D). However, ACh responses to VNS were significantly reduced during small whisk trials (mean = 0.08 ± 0.0008) compared to trials that triggered stronger whisking and wheel movement (mean = 0.37 ± 0.0017; $p < 0.0001$; Figures 4C and 4F). The magnitude of response of NA was significantly lower during anesthetized trials (mean = 0.33 ± 0.0009) compared to small whisk trials ($p < 0.05$), although VNS-evoked ACh signaling responded similarly during small whisk and anesthetized trials (mean = 0.05 ± 0.0005; $p = 0.80$). Finally, we tested whether NA or ACh axon activity may mediate the arousal response (as measured by pupil diameter) to VNS. We found a strong relationship between pupil diameter and NA signaling (mean regression parameter estimate [m] = 0.97; 95% confidence interval, 1,000 bootstrapped replicates [CI] = [0.48, 1.48]) and ACh (m = 0.42; CI = [0.17, 0.23]) that disappeared when mediation effects of NA or ACh axon activity were taken into account (NA: $m = 3.5 \times 10^{-5}$, CI = [-3.7×10^{-6}, 7.3×10^{-5}]; ACh: $m = 6.3 \times 10^{-5}$, CI = [-4.7×10^{-5}, 7.9×10^{-5}]; Figure S4).

DISCUSSION

VNS is a well-established treatment for a number of conditions,[1–4] but it is unclear what rapid physiological effects VNS has on brain activity. Here, we show that VNS exerts a prominent effect on arousal and brain state. In this study, VNS dose dependently increased three behavioral measures of arousal state: pupil dilation; whisker movements; and wheel movement (walking). In addition, we demonstrate that VNS leads to robust and widespread cortical activation. Finally, we present evidence that activity in the ascending noradrenergic and cholinergic neuromodulatory systems is increased in response to VNS. Our results support a model of VNS in which stimulation of the vagus nerve leads to activation of subcortical structures (e.g., the noradrenergic locus coeruleus and cholinergic basal forebrain) that send broad projections throughout the brain, contributing to activation of the cortex and a change in brain and behavioral state (Figure 4G).

VNS and arousal state

Arousal state during waking periods fluctuates on a moment-to-moment basis and robustly influences cortical processing and behavior.[22,31,32] Our results demonstrate that VNS indeed exerts a significant influence over arousal state. Application of VNS reliably resulted in pupil dilation, often coupled with facial/whisker pad movement and locomotion. The effect of VNS on arousal state was dose dependent such that increasing stimulus duration, pulse width, or current intensity increased the change in cortical and behavioral arousal. Importantly, these effects were extinguished after transection of the vagus nerve. Due to the location of the cuff electrode near large chest muscles, off-target stimulation of surrounding musculature with VNS is possible (especially during high-intensity stimulations); however, because transection nullified all effects on arousal, we are confident that the effects we observed of VNS on arousal state did not result from off-target (i.e., non-vagus nerve) stimulation (see also Mridha et al.[33]).

Variations in arousal significantly impact an animal's ability to perform behavioral tasks.[22,34] Performance on an auditory discrimination task has been shown to follow an "inverted-U" pattern, in which low and high levels of arousal negatively impact performance, whereas performance is best during intermediate arousal states.[22,35] In our study, the magnitude of arousal changes after VNS was dependent on the arousal state of the animal at the onset of VNS. VNS induced large changes in pupil diameter and evoked whisking and locomotion when applied during low arousal states (e.g., lack of movement and small pupil diameter). Conversely, VNS delivered during periods of locomotion resulted in relatively small increases in arousal (pupil dilation). Therefore, VNS delivery tended to shift animals toward an intermediate to high arousal state, except for periods of high arousal in which VNS had little effect. The observed state dependence of VNS application could be partially explained by a ceiling effect. At high arousal states, pupils are near maximum diameter, and therefore, the range of possible further increases is reduced. However, we noted a similar trend at submaximal arousal levels when maximal pupil dilation (e.g., the physical ceiling) was not reached during VNS (Figure 1C).

Some evidence suggests that VNS can evoke an arousal state change in humans in a vegetative or minimally conscious state;[36–38] however, we are unaware of any evidence that overt movements are induced in humans in a similar way that we observed in mice. Further work is needed to understand species differences in arousal responses to VNS.

Global changes in cortical activity

Because we observed large arousal state changes in response to VNS, we hypothesized that VNS would also induce significant cortical activation.[22,29,39,40] Indeed, VNS induced widespread

cortical activation that was similar to but distinct from that observed during spontaneous increases in arousal state.[24] Widespread, bilateral activation of motor, somatosensory, visual, and retrosplenial cortices was noted, alongside activation in the lateral auditory and barrel cortices during both VNS and spontaneous arousal and movement. However, in contrast to spontaneous increases in cortical activity, the spatiotemporal pattern of which is dependent upon behavioral state,[41] activation in response to VNS, although widespread, was centered on the lower limb/body area of somatosensory cortex (Figure 2C). The observed broad, bilateral cortical activation in response to VNS is likely due to bilateral activation of broadly projecting brainstem nuclei. There are multiple paths by which the activation of the vagus nerve could influence cortical activity, particularly at the timescales observed in the present study. For example, the vagus nerve conveys efferents from internal organs to brainstem nuclei on both sides (nucleus of the solitary tract, area postrema, and dorsal motor nucleus of the vagus nerve).[42] Efferents of the nucleus of the solitary tract synapse onto noradrenergic dendrites of the LC,[43] which in turn projects largely ipsilaterally to widespread regions of the cortex.[44]

This cortical activation was again found to be dose dependent. Low-intensity stimulations that evoked little to no arousal change similarly did not elicit detectable changes in cortical excitation, whereas high-intensity stimulations that induced pupil dilation, whisking, and/or wheel movement[33] also caused large increases in cortical neuronal calcium signaling. We controlled for the well-documented effect of motor activity on cortical excitation[45] by examining VNS applications that only evoked whisking or pupil dilation and by performing VNS experiments in lightly anesthetized mice. In the absence of any detectable motor activity as well as under light anesthesia, increased activity in GCaMP6s was still observed in the cortex in response to VNS, indicating that VNS can excite cortical circuits beyond that associated with motor activity. Moreover, fluorescence changes during VNS-induced locomotive bouts were greater than those observed during spontaneous locomotion, indicating that VNS and motor activity produce a distinct effect on cortical excitation. Such widespread spatial diversity of VNS-induced cortical activation demonstrates that VNS has broad effects throughout the brain and likely impacts cortical processing in myriad ways. Whether cortical excitation caused by VNS impacts neural circuits in similar ways across functional cortices or layers remains to be determined.

When examining individual excitatory cell activity using two-photon imaging, we found that VNS rapidly (within 1 s) recruits a substantial proportion of cortical excitatory neurons (87% and 64% when awake and under anesthesia, respectively). This mirrors the transient increase in firing rate noted using multi-unit recording in the same region. Interestingly, VNS did not induce a persistent increase in cortical firing rate throughout the duration of a longer 5-s stimulation train during applications that did not elicit walking. This suggests that the cortical activation evoked by VNS may be triggered by a rapid neuromodulatory activation that may become desensitized or depleted approximately 1 s after VNS onset. However, in trials that evoked walking or whisking behaviors, a longer lasting increase in multi-unit activity as well as widefield GCaMP6s signaling was observed, potentially reflecting increased cortical excitation accompanying bouts of motor activity. Interpretation of simultaneously collected physiological and behavioral data is complicated by the differing time courses on which each variable behaves. For example, pupil dilation is known to lag internal state changes mediated by LC, because pupil diameter is controlled by a smooth muscle.[46] Similarly, locomotion requires activation of pathways involving central and peripheral neurons before observable changes in behavior can be measured. However, these results coupled with the evidence from anesthetized mice described above strongly suggest that VNS induces a rapid, transient depolarization (activation) across the cortex, altering internal brain state and external behavioral state.

Neuromodulatory underpinnings of VNS effects

Anatomical and physiological studies have previously provided evidence that VNS may excite cortical neurons through neuromodulatory pathways, including those releasing ACh or NA.[11,47] Fibers carrying information from the vagus nerve synapse in the nucleus of the solitary tract then project to the noradrenergic LC. From the LC, projections are sent throughout the brain, including to subcortical structures, such as the basal forebrain (BF), thalamus, and cerebral cortex.[15,48] Cholinergic BF neuron projections are also widely dispersed throughout cortical and subcortical structures.[48,49] Both ACh and NA release into the cortex can produce excitatory effects. ACh can directly increase the excitability of pyramidal neurons and also disinhibit pyramidal cells through excitation of vasointestinal-peptide-expressing interneurons, which can inhibit both somatostatin and parvalbumin-containing interneurons, which typically project to the apical dendrites, somata, and axon hillocks of cortical pyramidal cells.[50–52] NA released in the cortex can exert either excitatory or inhibitory effects on cortical neurons, mediated by α1 and α2 G-protein-coupled receptors, respectively.[15]

Our results and others support a model of VNS in which stimulation activates multiple pathways, including both ACh and NA systems, and leads to excitation/activation of the cortex. The widespread cortical activation we observed hints that VNS induces arousal state changes via broadly projecting neuromodulatory systems, although the activation of more-specific direct glutamatergic excitatory pathways through the brainstem is also likely.[53,54] Within the LC, VNS dose dependently increases firing rate of neurons within 100 ms.[10] Indeed, our results demonstrate that the neurons activated in the LC project to the cortex, where we observed a strong activation of NA fibers following VNS. A similar observation has been made in the rat in which extracellular concentrations of NA in the cortex are increased following VNS.[47] We also detected an increase in ACh axonal cortical activity soon after VNS onset. Once again, a similar effect has been recorded in the anesthetized rat, where VNS acts via cholinergic muscarinic receptors to desynchronize ongoing cortical activity.[14] Together with these previous studies, our results clearly demonstrate that VNS robustly activates cholinergic and noradrenergic neurons that send widespread projections to the cortex.

Arousal state covaries with signaling of cholinergic and noradrenergic neurons.[16,17,30,31,55,56] We have shown that VNS initiates activity in these same neuromodulatory centers and that the extent to which ACh and NA activity increases in response to VNS is influenced by initiation of movement. Applications

that evoked whisking or walking behaviors resulted in greater activation of both ACh and NA axons than applications in which no motor activity was detected. However, some VNS-evoked increase in ACh and NA activity persists under light anesthesia in the absence of overt movement, so the observed effects of VNS on ACh and NA signaling cannot be explained by that associated with motor activity alone. We speculate that VNS can have a potent activating influence, even in the absence of overt movements, and that behavioral arousal (i.e., movements) can further amplify the activation of these neuromodulatory systems.

An inverted-U response pattern has been reported for cortical ACh activity[33] in response to increasing intensities of VNS; however, this same inverted-U response pattern is not present in LC neurons following VNS.[10] Similarly, enhancement of performance of behavioral tasks[57,58] and cortical map plasticity[59,60] is strongest in response to intermediate intensities of stimulation. These findings suggest a potential relationship between VNS-induced activation of neuromodulatory systems and learning. However, further investigation of dose-dependent activation of neuromodulatory systems is warranted to clarify the contribution of these systems on VNS-induced enhancement of learning.

Conclusions

Overall, our findings support the hypothesis that VNS increases arousal state and results in activation of the neocortex through mechanisms that include increases in activity in noradrenergic neurons in the LC and cholinergic neurons in the BF (Figure 4G). We note that the increased arousal state evoked by VNS often triggers further motor activity, which amplifies both excitatory and neuromodulatory signaling in the cortex. The influence that VNS has on arousal and these neuromodulatory systems may underpin, or contribute to, the therapeutic effects that VNS has on epilepsy and migraine, conditions which commonly have triggers related to sleep and waking states.[18,61–63] Perhaps enhanced learning and performance observed as a result of VNS delivery can also be partially explained by the optimization of arousal state.[64–66] Future studies investigating the precise doses and timing of VNS application may ultimately help to improve the therapeutic use of VNS for a number of conditions.

STAR★METHODS

Detailed methods are provided in the online version of this paper and include the following:

- KEY RESOURCES TABLE
- RESOURCE AVAILABILITY
  - Lead contact
  - Materials availability
  - Data and code availability
- EXPERIMENTAL MODEL AND SUBJECT DETAILS
  - Animals
- METHOD DETAILS
  - Surgical Procedures
  - Vagus Nerve Stimulation Parameters
  - Arousal Measures
  - Widefield Imaging
  - Multiunit recording
  - 2-photon Imaging
- QUANTIFICATION AND STATISTICAL ANALYSIS
  - Behavioral Data Analysis
  - Widefield Imaging Analysis
  - 2-Photon Imaging Analysis
  - Statistical Analysis

SUPPLEMENTAL INFORMATION

Supplemental information can be found online at https://doi.org/10.1016/j.cub.2021.02.049.

ACKNOWLEDGMENTS

We would like to thank the members of the McCormick lab for helpful discussions throughout this project and give a special thanks to Minh Nguyen, who assisted with analysis of cortical blood vessel data. We would also like to thank Matthew McGinley and Robert Froemke for helpful discussions related to this project. This work was funded by the Defense Advanced Research Projects Agency (DARPA) Targeted Neuroplasticity Training Program - BAA-16-24 and the National Institutes of Health (NIH) R35NS097287.

AUTHOR CONTRIBUTIONS

Conceptualization, L.B., L.C., and D.M.; Methodology, P.J.S., L.B., and L.C.; Investigation, L.B. and L.C.; Formal Analysis, L.B. and L.C.; Writing – Original Draft, L.B., L.C., and D.M.; Writing – Review & Editing, L.B., L.C., and D.M.; Visualization, L.B. and L.C.; Funding Acquisition, D.M.; Supervision, D.M.

DECLARATION OF INTERESTS

The authors declare no competing interests.

Received: January 1, 2021
Revised: February 1, 2021
Accepted: February 17, 2021
Published: March 18, 2021

REFERENCES

1. Sackeim, H.A., Rush, A.J., George, M.S., Marangell, L.B., Husain, M.M., Nahas, Z., Johnson, C.R., Seidman, S., Giller, C., Haines, S., et al. (2001). Vagus nerve stimulation (VNS) for treatment-resistant depression: efficacy, side effects, and predictors of outcome. Neuropsychopharmacology *25*, 713–728.
2. Groves, D.A., and Brown, V.J. (2005). Vagal nerve stimulation: a review of its applications and potential mechanisms that mediate its clinical effects. Neurosci. Biobehav. Rev. *29*, 493–500.
3. Englot, D.J., Chang, E.F., and Auguste, K.I. (2011). Efficacy of vagus nerve stimulation for epilepsy by patient age, epilepsy duration, and seizure type. Neurosurg. Clin. N. Am. *22*, 443–448, v.
4. Schwedt, T.J., and Vargas, B. (2015). Neurostimulation for treatment of migraine and cluster headache. Pain Med. *16*, 1827–1834.
5. De Ridder, D., Vanneste, S., Engineer, N.D., and Kilgard, M.P. (2014). Safety and efficacy of vagus nerve stimulation paired with tones for the treatment of tinnitus: a case series. Neuromodulation *17*, 170–179.
6. Dawson, J., Pierce, D., Dixit, A., Kimberley, T.J., Robertson, M., Tarver, B., Hilmi, O., McLean, J., Forbes, K., Kilgard, M.P., et al. (2016). Safety, feasibility, and efficacy of vagus nerve stimulation paired with upper-limb rehabilitation after ischemic stroke. Stroke *47*, 143–150.
7. Johnson, R.L., and Wilson, C.G. (2018). A review of vagus nerve stimulation as a therapeutic intervention. J. Inflamm. Res. *11*, 203–213.
8. Chae, J.-H., Nahas, Z., Lomarev, M., Denslow, S., Lorberbaum, J.P., Bohning, D.E., and George, M.S. (2003). A review of functional neuroimaging studies of vagus nerve stimulation (VNS). J. Psychiatr. Res. *37*, 443–455.

9. Cao, J., Lu, K.-H., Powley, T.L., and Liu, Z. (2017). Vagal nerve stimulation triggers widespread responses and alters large-scale functional connectivity in the rat brain. PLoS ONE *12*, e0189518.
10. Hulsey, D.R., Riley, J.R., Loerwald, K.W., Rennaker, R.L., 2nd, Kilgard, M.P., and Hays, S.A. (2017). Parametric characterization of neural activity in the locus coeruleus in response to vagus nerve stimulation. Exp. Neurol. *289*, 21–30.
11. Dorr, A.E., and Debonnel, G. (2006). Effect of vagus nerve stimulation on serotonergic and noradrenergic transmission. J. Pharmacol. Exp. Ther. *318*, 890–898.
12. Détári, L., Juhász, G., and Kukorelli, T. (1983). Effect of stimulation of vagal and radial nerves on neuronal activity in the basal forebrain area of anaesthetized cats. Acta Physiol. Hung. *61*, 147–154.
13. Hays, S.A. (2016). Enhancing rehabilitative therapies with vagus nerve stimulation. Neurotherapeutics *13*, 382–394.
14. Nichols, J.A., Nichols, A.R., Smirnakis, S.M., Engineer, N.D., Kilgard, M.P., and Atzori, M. (2011). Vagus nerve stimulation modulates cortical synchrony and excitability through the activation of muscarinic receptors. Neuroscience *189*, 207–214.
15. Rho, H.-J., Kim, J.-H., and Lee, S.-H. (2018). Function of selective neuromodulatory projections in the mammalian cerebral cortex: comparison between cholinergic and noradrenergic systems. Front. Neural Circuits *12*, 47.
16. Joshi, S., Li, Y., Kalwani, R.M., and Gold, J.I. (2016). Relationships between pupil diameter and neuronal activity in the locus coeruleus, colliculi, and cingulate cortex. Neuron *89*, 221–234.
17. Reimer, J., Froudarakis, E., Cadwell, C.R., Yatsenko, D., Denfield, G.H., and Tolias, A.S. (2014). Pupil fluctuations track fast switching of cortical states during quiet wakefulness. Neuron *84*, 355–362.
18. Della Marca, G., Vollono, C., Rubino, M., Di Trapani, G., Mariotti, P., and Tonali, P.A. (2006). Dysfunction of arousal systems in sleep-related migraine without aura. Cephalalgia *26*, 857–864.
19. Thase, M.E. (2006). Depression and sleep: pathophysiology and treatment. Dialogues Clin. Neurosci. *8*, 217–226.
20. Ewell, L.A., Liang, L., Armstrong, C., Soltész, I., Leutgeb, S., and Leutgeb, J.K. (2015). Brain state is a major factor in preseizure hippocampal network activity and influences success of seizure intervention. J. Neurosci. *35*, 15635–15648.
21. Hulsey, D.R., Shedd, C.M., Sarker, S.F., Kilgard, M.P., and Hays, S.A. (2019). Norepinephrine and serotonin are required for vagus nerve stimulation directed cortical plasticity. Exp. Neurol. *320*, 112975.
22. McGinley, M.J., David, S.V., and McCormick, D.A. (2015). Cortical membrane potential signature of optimal states for sensory signal detection. Neuron *87*, 179–192.
23. Musall, S., Kaufman, M.T., Juavinett, A.L., Gluf, S., and Churchland, A.K. (2019). Single-trial neural dynamics are dominated by richly varied movements. Nat. Neurosci. *22*, 1677–1686.
24. Salkoff, D.B., Zagha, E., McCarthy, E., and McCormick, D.A. (2020). Movement and performance explain widespread cortical activity in a visual detection task. Cereb. Cortex *30*, 421–437.
25. Stringer, C., Pachitariu, M., Steinmetz, N., Reddy, C.B., Carandini, M., and Harris, K.D. (2019). Spontaneous behaviors drive multidimensional, brain-wide activity. Science *364*, 255.
26. Ma, Y., Thibodeaux, D.N., Shaik, M.A., Kim, S.H., and Hillman, E.M.C. (2017). Wide-field optical mapping of neural activity in awake mice and the importance of hemodynamic correction. In Optics in the Life Sciences Congress (OSA), BrS1B.3.
27. Chen, T.-W., Wardill, T.J., Sun, Y., Pulver, S.R., Renninger, S.L., Baohan, A., Schreiter, E.R., Kerr, R.A., Orger, M.B., Jayaraman, V., et al. (2013). Ultrasensitive fluorescent proteins for imaging neuronal activity. Nature *499*, 295–300.
28. Wekselblatt, J.B., Flister, E.D., Piscopo, D.M., and Niell, C.M. (2016). Large-scale imaging of cortical dynamics during sensory perception and behavior. J. Neurophysiol. *115*, 2852–2866.
29. Reimer, J., McGinley, M.J., Liu, Y., Rodenkirch, C., Wang, Q., McCormick, D.A., and Tolias, A.S. (2016). Pupil fluctuations track rapid changes in adrenergic and cholinergic activity in cortex. Nat. Commun. *7*, 13289.
30. Eggermann, E., Kremer, Y., Crochet, S., and Petersen, C.C.H. (2014). Cholinergic signals in mouse barrel cortex during active whisker sensing. Cell Rep. *9*, 1654–1660.
31. Larsen, R.S., and Waters, J. (2018). Neuromodulatory correlates of pupil dilation. Front. Neural Circuits *12*, 21.
32. McCormick, D.A., Nestvogel, D.B., and He, B.J. (2020). Neuromodulation of brain state and behavior. Annu. Rev. Neurosci. *43*, 391–415.
33. Mridha, Z., de Gee, J.W., Shi, Y., Alkashgari, R., Williams, J., Suminski, A., Ward, M.P., Zhang, W., and McGinley, M.J. (2019). Graded recruitment of pupil-linked neuromodulation by parametric stimulation of the vagus nerve. bioRxiv. https://doi.org/10.1101/2019.12.28.890111.
34. Neske, G.T., Nestvogel, D., Steffan, P.J., and McCormick, D.A. (2019). Distinct waking states for strong evoked responses in primary visual cortex and optimal visual detection performance. J. Neurosci. *39*, 10044–10059.
35. Waschke, L., Tune, S., and Obleser, J. (2019). Local cortical desynchronization and pupil-linked arousal differentially shape brain states for optimal sensory performance. eLife *8*, e51501.
36. Corazzol, M., Lio, G., Lefevre, A., Deiana, G., Tell, L., André-Obadia, N., Bourdillon, P., Guenot, M., Desmurget, M., Luauté, J., and Sirigu, A. (2017). Restoring consciousness with vagus nerve stimulation. Curr. Biol. *27*, R994–R996.
37. Yu, Y.-T., Yang, Y., Wang, L.-B., Fang, J.-L., Chen, Y.-Y., He, J.-H., and Rong, P.-J. (2017). Transcutaneous auricular vagus nerve stimulation in disorders of consciousness monitored by fMRI: The first case report. Brain Stimul. *10*, 328–330.
38. Xiang, X.-J., Sun, L.-Z., Xu, C.-B., Xie, Y., Pan, M.-Y., Ran, J., Hu, Y., Nong, B.-X., Shen, Q., Huang, H., et al. (2020). The clinical effect of vagus nerve stimulation in the treatment of patients with a minimally conscious state. J. Neurorestoratol. *8*, 160–171.
39. Constantinople, C.M., and Bruno, R.M. (2011). Effects and mechanisms of wakefulness on local cortical networks. Neuron *69*, 1061–1068.
40. Vinck, M., Batista-Brito, R., Knoblich, U., and Cardin, J.A. (2015). Arousal and locomotion make distinct contributions to cortical activity patterns and visual encoding. Neuron *86*, 740–754.
41. West, S.L., Aronson, J., Popa, L.S., Carter, R.E., Shekhar, A., Feller, K.D., Ghanbari, L., Kodandaramaiah, S.B., and Ebner, T.J. (2020). Wide-field calcium imaging of dynamic cortical networks during locomotion. bioRxiv. https://doi.org/10.1101/2020.07.06.189670.
42. Kalia, M., and Sullivan, J.M. (1982). Brainstem projections of sensory and motor components of the vagus nerve in the rat. J. Comp. Neurol. *211*, 248–265.
43. Van Bockstaele, E.J., Peoples, J., and Telegan, P. (1999). Efferent projections of the nucleus of the solitary tract to peri-locus coeruleus dendrites in rat brain: evidence for a monosynaptic pathway. J. Comp. Neurol. *412*, 410–428.
44. Toussay, X., Basu, K., Lacoste, B., and Hamel, E. (2013). Locus coeruleus stimulation recruits a broad cortical neuronal network and increases cortical perfusion. J. Neurosci. *33*, 3390–3401.
45. Niell, C.M., and Stryker, M.P. (2010). Modulation of visual responses by behavioral state in mouse visual cortex. Neuron *65*, 472–479.
46. Liu, Y., Rodenkirch, C., Moskowitz, N., Schriver, B., and Wang, Q. (2017). Dynamic lateralization of pupil dilation evoked by locus coeruleus activation results from sympathetic, not parasympathetic, contributions. Cell Rep. *20*, 3099–3112.
47. Roosevelt, R.W., Smith, D.C., Clough, R.W., Jensen, R.A., and Browning, R.A. (2006). Increased extracellular concentrations of norepinephrine in cortex and hippocampus following vagus nerve stimulation in the rat. Brain Res. *1119*, 124–132.
48. Kim, J.-H., Jung, A.-H., Jeong, D., Choi, I., Kim, K., Shin, S., Kim, S.J., and Lee, S.-H. (2016). Selectivity of neuromodulatory projections from the

basal forebrain and locus ceruleus to primary sensory cortices. J. Neurosci. *36*, 5314–5327.

49. Schwarz, L.A., Miyamichi, K., Gao, X.J., Beier, K.T., Weissbourd, B., DeLoach, K.E., Ren, J., Ibanes, S., Malenka, R.C., Kremer, E.J., and Luo, L. (2015). Viral-genetic tracing of the input-output organization of a central noradrenaline circuit. Nature *524*, 88–92.
50. Metherate, R., Cox, C.L., and Ashe, J.H. (1992). Cellular bases of neocortical activation: modulation of neural oscillations by the nucleus basalis and endogenous acetylcholine. J. Neurosci. *12*, 4701–4711.
51. Hedrick, T., and Waters, J. (2015). Acetylcholine excites neocortical pyramidal neurons via nicotinic receptors. J. Neurophysiol. *113*, 2195–2209.
52. Dasgupta, R., Seibt, F., and Beierlein, M. (2018). Synaptic release of acetylcholine rapidly suppresses cortical activity by recruiting muscarinic receptors in layer 4. J. Neurosci. *38*, 5338–5350.
53. Fung, S.J., Reddy, V.K., Liu, R.H., Wang, Z., and Barnes, C.D. (1994). Existence of glutamate in noradrenergic locus coeruleus neurons of rodents. Brain Res. Bull. *35*, 505–512.
54. Liu, R.-H., Fung, S.J., Reddy, V.K., and Barnes, C.D. (1995). Localization of glutamatergic neurons in the dorsolateral pontine tegmentum projecting to the spinal cord of the cat with a proposed role of glutamate on lumbar motoneuron activity. Neuroscience *64*, 193–208.
55. de Gee, J.W., Colizoli, O., Kloosterman, N.A., Knapen, T., Nieuwenhuis, S., and Donner, T.H. (2017). Dynamic modulation of decision biases by brainstem arousal systems. eLife *6*, e23232.
56. Breton-Provencher, V., and Sur, M. (2019). Active control of arousal by a locus coeruleus GABAergic circuit. Nat. Neurosci. *22*, 218–228.
57. Clark, K.B., Naritoku, D.K., Smith, D.C., Browning, R.A., and Jensen, R.A. (1999). Enhanced recognition memory following vagus nerve stimulation in human subjects. Nat. Neurosci. *2*, 94–98.
58. Clark, K.B., Krahl, S.E., Smith, D.C., and Jensen, R.A. (1995). Post-training unilateral vagal stimulation enhances retention performance in the rat. Neurobiol. Learn. Mem. *63*, 213–216.
59. Morrison, R.A., Hulsey, D.R., Adcock, K.S., Rennaker, R.L., 2nd, Kilgard, M.P., and Hays, S.A. (2019). Vagus nerve stimulation intensity influences motor cortex plasticity. Brain Stimul. *12*, 256–262.
60. Borland, M.S., Vrana, W.A., Moreno, N.A., Fogarty, E.A., Buell, E.P., Sharma, P., Engineer, C.T., and Kilgard, M.P. (2016). Cortical map plasticity as a function of vagus nerve stimulation intensity. Brain Stimul. *9*, 117–123.
61. Sedigh-Sarvestani, M., Thuku, G.I., Sunderam, S., Parkar, A., Weinstein, S.L., Schiff, S.J., and Gluckman, B.J. (2014). Rapid eye movement sleep and hippocampal theta oscillations precede seizure onset in the tetanus toxin model of temporal lobe epilepsy. J. Neurosci. *34*, 1105–1114.
62. Sedigh-Sarvestani, M., Blumenfeld, H., Loddenkemper, T., and Bateman, L.M. (2015). Seizures and brain regulatory systems: consciousness, sleep, and autonomic systems. J. Clin. Neurophysiol. *32*, 188–193.
63. Gumusyayla, S., Erdal, A., Tezer, F.I., and Saygi, S. (2016). The temporal relation between seizure onset and arousal-awakening in temporal lobe seizures. Seizure *39*, 24–27.
64. Lai, J., and David, S.V. (2019). Short-term effects of vagus nerve stimulation on learning and evoked activity in auditory cortex. bioRxiv. https://doi.org/10.1101/2019.12.19.883165.
65. Ghacibeh, G.A., Shenker, J.I., Shenal, B., Uthman, B.M., and Heilman, K.M. (2006). The influence of vagus nerve stimulation on memory. Cogn. Behav. Neurol. *19*, 119–122.
66. Sun, L., Peräkylä, J., Holm, K., Haapasalo, J., Lehtimäki, K., Ogawa, K.H., Peltola, J., and Hartikainen, K.M. (2017). Vagus nerve stimulation improves working memory performance. J. Clin. Exp. Neuropsychol. *39*, 954–964.
67. Pachitariu, M., Stringer, C., Dipoppa, M., Schröder, S., Rossi, L.F., Dalgleish, H., Carandini, M., and Harris, K.D. (2017). Suite2p: beyond 10,000 neurons with standard two-photon microscopy. bioRxiv. https://doi.org/10.1101/061507.
68. Sofroniew, N.J., Flickinger, D., King, J., and Svoboda, K. (2016). A large field of view two-photon mesoscope with subcellular resolution for in vivo imaging. eLife *5*, e14472.
69. Bakker, R., Tiesinga, P., and Kötter, R. (2015). The Scalable Brain Atlas: instant web-based access to public brain atlases and related content. Neuroinformatics *13*, 353–366.

STAR★METHODS

KEY RESOURCES TABLE

REAGENT or RESOURCE	SOURCE	IDENTIFIER
Experimental models: organisms/strains		
Mouse: Thy1-GCamp6s: Tg(Thy1-GCaMP6s)GP4.3Dkim	The Jackson Laboratory	IMSR Cat# JAX:024275; RRID: IMSR_JAX:024275
Mouse: CaMKII-GCaMP6s: Tg(tetO-GCaMP6s)2Niell	The Jackson Laboratory	IMSR Cat# JAX:024742; RRID: IMSR_JAX:024742
Mouse: ChAT-cre: Chattm2(cre)Lowl	The Jackson Laboratory	IMSR Cat# JAX:006410; RRID: IMSR_JAX:006410
Mouse: DBH-cre: Dbhtm3.2(cre)Pjen	The Jackson Laboratory	IMSR Cat# JAX:033951; RRID: IMSR_JAX:033951
Mouse: Ai162: Igs7tm162.1(tetO-GCaMP6s,CAG-tTA2)Hze	The Jackson Laboratory	IMSR Cat# JAX:031562; RRID: IMSR_JAX:031562
Software and algorithms		
Suite2P	[67]	https://github.com/MouseLand/suite2p
Other		
Resource website for this publication	This paper	https://github.com/lncollins91/VNS

RESOURCE AVAILABILITY

Lead contact

Further information and requests for resources should be directed to and will be fulfilled by the Lead Contact, David McCormick (davidmc@uoregon.edu).

Materials availability

This study did not generate new unique reagents.

Data and code availability

The codes generated during this study are available at https://github.com/lncollins91/VNS.

EXPERIMENTAL MODEL AND SUBJECT DETAILS

Animals

All experiments were approved by the University of Oregon Institutional Animal Care and Use Committee. Experiments were conducted using a total of 25 mice (16 male, 9 female) aged older than 7 weeks at study onset. All mouse strains used in this study were of C56BL/6J (IMSR Cat# JAX:000664, RRID: IMSR_JAX:000664) background and were purchased from Jackson Laboratory and bred in-house. Thy-1-GCamp6s (IMSR Cat# JAX:024275, RRID: IMSR_JAX:024275) were used for widefield imaging and electrophysiology studies. CaMKII-GCaMP6s (IMSR Cat# JAX:024742, RRID: IMSR_JAX:024742), ChAT-cre (IMSR Cat# JAX:006410, RRID: IMSR_JAX:006410) crossed with Ai162 (IMSR Cat# JAX:031562, RRID: IMSR_JAX:031562) and DBH-cre (IMSR Cat# JAX:033951, RRID: IMSR_JAX:033951) crossed with Ai162 mice were used for 2-photon imaging studies. All mice were individually housed under an inverted 12:12 hr light/dark regime and had access to food and water *ad libitum*. All experiments were conducted during the active dark cycle.

METHOD DETAILS

Surgical Procedures

All surgical procedures were performed in an aseptic environment with mice under 1%–2% isoflurane anesthesia (oxygen flow rate: > 1 L/min) and homeothermically maintained at 37.5°C. For vagus cuff implantation; under local (bupivacaine; 1%, s.c) and systemic analgesia (Meloxicam SR: 6 mg/kg, s.c.; Buprenorphine: 0.1 mg/kg, s.c.) a near-midline incision was made on the ventral aspect of the neck (Figure 1A). The submaxillary gland and connective tissue overlying the left cervical vagus nerve was retracted, and the nerve was isolated from the vessels within the carotid sheath. The cuff electrode was placed and secured around the nerve and the leads of a custom built cuff electrode were tunneled subcutaneously to an incision in the scalp. A suture was loosely tied across

the sternohyoid and sternomastoid muscles to secure the cuff electrode in place, and finally the neck incision was sutured closed. Next, the skin and connective tissue on the surface of the skull was removed and the exposed skull was cleaned. One of two custom-designed headplates (one for dorsal cortical surface imaging, the other for lateral cortical surface imaging) was affixed to the skull using dental cement (RelyX UniCem Aplicap, 3M) and the gold amphenol pins of the cuff electrode lead wires were affixed to the headplate with cyanoacrylate.

For widefield imaging, a layer of cyanoacrylate (Slow-Zap) was evenly applied to the skull to clear the skull bone. A layer of Kwik-Sil silicone was applied to protect the imaging field. For 2-photon imaging, instead of applying a layer of cyanoacrylate to clear the skull, an 8 mm circular craniotomy was made overlying the dorsal cortex using a dental drill. An 8 mm circular glass coverslip was placed in the craniotomy and the coverslip was affixed to the skull with Flow-It composite (Flow-It ALC, Pentron) and a thin layer of dental cement around the edges of the glass. After all surgeries, mice recovered for at least 1 hour in a ~85°F recovery chamber and post-operative Buprenorphine (0.1 mg/kg, s.c.) and warmed lactated ringer's solution was administered for 1 – 3 days, as required.

Following imaging experiments, some mice underwent a vagus nerve transection surgery. Surgical procedures (analgesics, anesthetics, neck incision, and nerve isolation) were identical to nerve cuff implantation, described above. Once the nerve and cuff were isolated transections were made using fine-tipped scissors. One nerve transection was made anterior to the placement of the cuff and another transection was made posterior to the cuff to block both afferent and efferent signaling through the vagus nerve. Each mouse received both proximal and distal transections in the same surgery. The neck incision was then sutured closed and the animal was allowed to recover in the same manner as described above.

Vagus Nerve Stimulation Parameters

The gold pins of the cuff electrode were connected to a programmable stimulus isolator (AM-Systems Model 2200) and VNS was triggered using custom Labview software. To determine optimal stimulation parameters VNS was delivered in blocked trials for either 5, 1, or 0.5 s at 30 Hz, at intensities of 100, 400, 800, or 1000 μA, with a pulse width of either 100, 500 or 800 μs.[33] Typical stimulation parameters shown in figures and throughout the text are 30 Hz, at 800 μA, for 1 s, with a pulse width of 800 μs, unless otherwise stated. Neither facial nor muscle twitching (an indication of off-target stimulation of musculature surrounding the vagus nerve) was observed with any parameters used in any of the mice included in the present study.

Arousal Measures

For all experiments, mice were head-fixed atop a cylindrical running wheel and video of the mouse face and pupil was acquired from the side at 30 Hz (Teledyne camera; Figure 1A). Pupil diameter was measured both in real-time and offline using a custom Labview script. Walking speed was measured using a rotary encoder (McMaster-Carr) attached to the wheel, and walking bouts were defined as moments when wheel velocity exceeded 2.5 cm/s for more than 1 s. Whisker-pad movement was measured by selecting a region of interest (approximately 1 × 1 cm) over the mystacial whisker pad containing the macrovibrissae and calculating the motion energy (ME) across the video. ME was defined as the sum of the absolute change in pixel intensity within the ROI between adjacent video frames. All waveform and trigger signals were digitized through either a Micro 1401 or Power 1401 and collected using Spike2 version 7 or 8 (Cambridge Electronic Design Limited).

Widefield Imaging

Widefield imaging was conducted as previously described.[24] Briefly, Thy-1-GCamp6s mice were head-fixed underneath a macroscope with a 75 mm lens (RedShirt Imaging, Macroscope-IIA; 4.5 f; NA 0.4) positioned on an air-table to limit movement artifacts. The transparent skull (see Surgical Procedures for details) was illuminated using a blue 490 nm mounted LED (Thorlabs M490 L4, LEDD1B) and dispersed with a collimating lens (Thorlabs ACL2520-A). The 490 nm light passed through a 470 nm bandpass filter (ET470/40x, Chroma) and a 495 nm long-pass dichroic mirror (T495lpxr, Chroma). After excitation of the GCaMP6s, the returning light was passed through a 510 nm bandpass filter (ET510–32 mm, Chroma) prior to entering the DaVinci 2K CMOS camera (RedShirt Imaging). Pixels were binned 2 × 2 for a final resolution of approximately 30 μm/binned pixel. Images were collected at 50 Hz, recorded using Red-Shirt Imaging Turbo-SM camera software, and triggered using custom Labview software. In a set of experiments, the hemodynamic signal was removed by subtracting the green reflectance recorded in every alternate frame.[26] A green 530 nm LED (Thorlabs LEDC13) and a collimating lens were mounted on the air-table and aimed at the surface of the skull. Alternating blue/green light was triggered using LED drivers (Thorlabs LEDD1B) and an Arduino microcontroller.

Multiunit recording

Multiunit recording was conducted from the center of the region of somatosensory cortex which showed the strongest activation under widefield imaging. After identification of this region a small 1 - 2 mm craniotomy was drilled under isoflurane anesthesia several hours prior to recording. Once animals had fully recovered from anesthesia the mice were mounted on the wheel. A tungsten microelectrode (1 MΩ impedance, FHC) was positioned in layer 2/3 using a micromanipulator (Sutter Instruments). Microelectrodes were coupled to a headstage (model #3000, AM Systems), which was further coupled to a single-channel amplifier (model #3000, AM Systems). Extracellular signals were amplified (1000x) and filtered (0.1 Hz to 20 kHz) by the single-channel amplifier and digitized at 20 kHz with the Micro1401 MKII data acquisition system (CED) and Spike2 data acquisition software (CED). LFP and MUA signals were acquired by filtering the raw extracellular signal from 0.1 to 300 Hz and from 300 Hz to 20 kHz, respectively. The tungsten electrode was lowered rapidly into the brain to layer 2/3 and then stepped slowly in 2-5 μm increments until multiunit activity was detected. VNS

was then applied in the same manner as previously described. VNS-evoked stimulus artifacts were detected and blanked offline. Action potentials were defined as events that exceeded 4x the standard deviation of the noise floor in extracellular signals (filtered from 300 Hz to 20 kHz) and were detected using custom MATLAB software. Normalized spike rate (multiunit spikes per 100 ms) was calculated and activity 2 s before and 7 s after VNS onset was analyzed.

2-photon Imaging

2-photon imaging was conducted using a ThorLabs Multiphoton Mesoscope (excitation NA 0.6, collection NA 1.0) equipped with a 12 kHz resonant scanner and virtually conjugated galvo scanner set along with a 1 mm range remote focusing unit, allowing for rapid imaging across multiple ROIs varying in X, Y, and Z coordinates simultaneously.[68] Excitation of GCaMP6s was achieved via a Ti-sapphire laser tuned to 920 nm (MaiTai, Spectra Physics). Scan Image software (Vidrio) was used for all imaging sessions. For cell body imaging a minimum resolution of 1 μm/pixel was used and for axonal imaging a minimum resolution of 0.5 μm/pixel was used to clearly delineate borders of somas or axonal processes. Images were collected at a minimum frequency of 10 Hz, in order to capture all available information about intracellular calcium concentration from GCaMP6s dynamics.[27]

QUANTIFICATION AND STATISTICAL ANALYSIS

Behavioral Data Analysis

All imaging data was aligned to behavioral data using custom MATLAB scripts. Pupil size is presented as a percentage of the maximum pupil diameter during each recording session. Maximal pupil diameter typically occurs during a prolonged bout of locomotion.[22] Percent change in pupil diameter after VNS onset was calculated as the average percent change of the pupil diameter during the 3 s after VNS onset in comparison to the average pupil diameter in the 1 s immediately preceding VNS.

Widefield Imaging Analysis

Widefield images of the dorsal surface were aligned to the Allen institute common coordinate framework (CCF) map[69] using structural landmarks and MATLAB code developed by Drs. Matt Kaufman and Shreya Saxena. Images from the lateral surface were aligned to the Allen Institute CCF map manually using tone-evoked responses and whisker pad movement to align auditory and barrel field regions. Widefield fluorescence signals were normalized pixel by pixel by the following equation $\Delta F/F = (F_i - F_0)/F_0$, where F_i is the raw fluorescence of the ith video frame, and F_0 is the mean of the lowest 10th percentile of signals for the entire video. For hemodynamic correction, hemodynamic signals from green light presentation were subtracted from the preceding blue light-evoked (GCaMP6s) fluorescence frame.

2-Photon Imaging Analysis

Suite2P[67] was used to identify cells and axons from 2-photon mesoscope imaging data. Pre-processing of calcium fluorescence data was performed using methods previously described.[29] Briefly, all traces were upsampled to 100 Hz and lowpass filtered to 10 Hz. Signal-to-noise ratios were then calculated for all traces by dividing the max power between the frequency range of 0.05-0.5 Hz by the mean power between 1-3 Hz. All traces that did not meet a minimum signal-to-noise criteria of log(20) were excluded from further analyses. Normalized fluorescence values were used in statistical analyses to avoid over-weighting larger or brighter axon segments. For displaying data, ΔF/F was calculated using the median fluorescence value over each recording session as the baseline fluorescence. All analyses were performed using custom MATLAB scripts, available at https://github.com/lncollins91/VNS.

Statistical Analysis

All group data are presented as mean (M) and standard error of the mean (SEM), unless otherwise stated. All statistical tests performed are notated throughout the text.